Impact of Hierarchization on the Textural Properties of MCM-22 Based Zeolites

Alexander Sachse, Thibaud Aumond, Julie Rousseau, Isabelle Batonneau-gener

Impact of hierarchization on the textural properties of MCM-22 based zeolites

Alexander Sachse, Thibaud Aumond, Julie Rousseau and Isabelle Batonneau-Gener*

Institut de Chimie des Milieux et Matériaux de Poitiers (IC2MP), Université de Poitiers – UMR 7285 CNRS, UFR SFA, Bat. B27, 4 rue Michel Brunet, TSA 51106, 86073 Poitiers, Cedex 9, France.

*corresponding author: alexander.sachse@univ-poitiers.fr

Abstract

The impact of zeolite hierarchization is often highlighted in terms of increased mesopore volume or specific surface area and preservation of micropore volume. Yet, though these targets may be achieved the accessibility to certain micropores might be negatively affected during hierarchization. A set of hierarchical MCM-22 based materials was prepared based on desilication treatments of MCM-22, of the layered precursor MCM-22(P) and of the CTAB swollen precursor swMCM-22(P) and by the pillaring of swMCM-22(P) leading to MCM-36. A new methodology was elaborated, which is based on comparing the micropore volume of pristine materials and *n*-nonane retaining samples. A definition of the accessible micropore volume fraction is given, which relates to the amount of surface 12-MR cups. This approach hence allows to quantify which type of microporosity is preferentially destroyed during hierarchization treatments of MCM-22. Besides comparing the development of mesoporosity, specific surface area and the evolution of micropore volume during hierarchization treatments the accessible micropore volume fraction allows for a distinct definition of the hierarchization quality for MCM-22 based materials. Despite an important increase in interlayer-mesopore volume and specific surface area for MCM-36 the accessible micropore volume fraction was found to be just 3% higher than for MCM-22.

Keywords: MCM-22, zeolite, mesopore, hierarchical, accessible

1. Introduction

Out of the known 253 zeolite frameworks the MWW structure is undoubtedly one of the most intriguing. MWW structured zeolites, such as MCM-22, feature a peculiar pore system that is composed of three independent domains.[1] Within the MCM-22 crystals two of these systems alternate, which can be described as: (*i*) 2D sinusoidal 10-Membered Ring (MR) channels (0.40 x 0.59 nm) and (*ii*) supercages (0.71 x 1.82 nm), which are connected in the *ab*-plane through non-circular 10-ring apertures (0.40 x 0.54 nm). These latter supercages are hence accessible only through the narrow 10-MRs. The third domain is encountered on the crystal surface and can be described as cups (or hemicages) featuring 12-MR openings (0.71 nm) of 0.70 nm depth.

MCM-22 based materials feature interesting catalytic properties and are industrially exploited in the alkylation of benzene in the Mobil–Badger EBMax and in the Mobil-Badger cumene processes.[2] The introduction of MCM-22 as acid catalyst indeed revolutionized these processes allowing to boost mono-alkylation selectivity and permitting conspicuous catalyst stability. The origin of these unparalleled catalytic properties is related to the unique textural properties of MCM-22 and notably to the presence of hemicages on the crystal surface.[3,4] Various synthetic pathways have been disclosed allowing to achieve distinct members of the MCM-22 family.[5] These are either achieved through direct synthesis or through post-synthetic modification of the lamellar MCM-22(P) precursor. Calcination of MCM-22(P) triggers the condensation of surface silanol groups leading to the 3D zeolite, named MCM-22.[6] Alternatively, the equivalent material can be achieved through direct synthesis and is known as MCM-49.[7] The swelling of the interlayer space of MCM-22(P) by cationic surfactants allows for the design of two further members of the MCM-22 family. Delamination of the swollen precursor leads to the singular ITQ-2 material, which can be described as disordered assembly of MCM-22 monolayers.[8] Moreover, the increased

interlayer space of the swollen MCM-22(P) can be stabilized through the introduction of silica pillars between the layers, leading to what is known as MCM-36, featuring interlayer-mesopores (2.5-3.0 nm).[9]

The development of hierarchical zeolites represents a sound solution in the quest to tailor their mass transfer properties.[10] Zeolite hierarchization allows for decreasing the diffusion path length, which has important implications in catalysis as the latter directly impacts the efficiency factor of a given process.[11] This moreover affects catalyst stability through reducing secondary reactions, which might lead to the development of deactivating species (*e.g.* coke).[12] An addition benefit of zeolite hierarchization is the possibility to increase the accessibility for bulky molecules to the zeolite active sites. This latter finds particular resonance as zeolites are believed to play an important role in the conversion of bio-sourced molecules into added-value products in future bio-refineries.[13]

In comparison to other zeolites, rather little has been reported on the hierarchization of MCM-22 materials. Various groups reported the achievement of hierarchical MCM-22 based on post-synthetic alkaline treatments.[14-16] The development of intracrystalline porosity allowed in these cases for achieving superior catalytic outputs. Surfactant-assisted post-synthetic desilication was further reported for MCM-49 and MCM-22.[17,18] Here again increased stability and activity in alkylation and acetalization reactions was observed. The achievement of modified MCM-22 was further reported through the use of organosilanes during synthesis.[19] Superior activity was referred for the glycerol condensation, which was ascribed to increased accessibility to active sites and to a higher hydrophobicity degree in the hierarchical sample. Further post-synthetic modifications based on dealumination were reported, which were yet conducted with the scope to selectively remove active sites from the supercages.[20]

The impact of such post-synthetic treatments on the distinct pore systems has up to date only scarcely been approached. This yet might be of fundamental importance, as active sites located in different pore environments present distinct catalytic properties as indicated by Guisnet and co-workers.[4] The authors achieved insights by selectively poisoning acid sites located in the hemicages through the interaction with the bulky base 2,4-dimethylquinoleine, which entrance to 10-MRs is sterically hindered. By comparing the product distributions of the *m*-xylene transformation on pristine MCM-22 and on hemicage poisoned MCM-22 the authors were able to observe important selectivity differences, which could be related to the different topologies of the various pore systems. Such a methodology is of great interest for understanding the role of acid sites in different topological environments; from a textural point of view the use of bulky bases is yet not satisfactory, as: (*i*) the distribution and amount of acid sites may be very heterogeneous within the distinct pore systems, (*ii*) the acidity might be impacted by the presence of extraframework alumina or silica species and (*iii*) the methodology is only useful for MCM-22 based materials that feature sufficient amount and strength of acid sites and is there for futile for MCM-22 zeotypes, featuring heteroatoms such as Ti or B or even for the MCM-22 all-silica counterpart ITQ-1.

In this contribution we report the impact of hierarchization through alkaline treatment on different MCM-22 type materials. Hierarchization strategies are qualified by comparing the amount of preserved micropore volume and by contrasting the development of mesopore volume and specific surface area. A new methodological approach is further presented based on comparing nitrogen physisorption isotherms of hierarchical MCM-22 based materials and of the *n*-nonane retaining counterparts, which allows for calculating the accessible micropore volume fraction (φ_{N_2}) and hence permits for defining hierarchization quality from a novel point of view and allows to quantify the type of microporosity that is preferentially removed during hierarchization.

2. Results and discussion

2.1 Definition of the accessible micropore volume fraction

The *n*-nonane (nC_9) adsorption and desorption isotherm on MCM-22 at ambient temperature (RT) allows to observe a steep increase of nC_9 amount at low relative pressures corresponding to the micropore filling (**Figure 1a**). Further nC_9 uptake is related to the adsorption on the outer surface of the crystals and to condensation in intercrystalline voids at higher relative pressure. The TEM images of MCM-22 indeed reveal agglomerates of crystals featuring plate-like morphology with dimensions ranging from 100 – 300 nm and of approximately 10 nm thickness (**Figure 2**). The desorption branch of the nC_9 isotherm closes the adsorption branch at a relative pressure of 0.35. Yet, in the micropore region (at low relative pressure) desorption deviates again from the adsorption branch and is incomplete even after evacuating the sample under secondary vacuum (1×10^{-4} mbar) during 72 h (**Figure 1b**). This observation indicates that the nC_9 desorption from MCM-22 is to a certain extent thermodynamically hindered and a given nC_9 amount (0.484 mmol g^{-1}) remains adsorbed within the micropores (red line in **Figure 1b**). Samples obtained after incomplete nC_9 desorption will hereafter be referred as nC_9 retaining materials.

To further investigate the porous structure nitrogen physisorption isotherms at 77 K were recorded for MCM-22 and for the nC_9 retaining MCM-22 (*i.e.* MCM-22-nC_9), (**Figure 1c**). As expected both isotherms feature a similar shape. The nitrogen uptake is yet significantly lower for MCM-22-nC_9 indicating that an important portion of the micropore volume is inaccessible to nitrogen. For MCM-22 and MCM-22-nC_9 a micropore volume of 0.166 and 0.046 $cm^3\ g^{-1}$ was respectively calculated. Hence, 0.120 $cm^3\ g^{-1}$ of the micropore volume is blocked by confined nC_9. By comparing the retained amount of nC_9 in MCM-22-nC_9 (*i.e.* 0.484 mmol g^{-1}) with the inaccessible micropore volume deduced by comparing N_2 physisorption isotherms (*i.e.* 0.120 $cm^3\ g^{-1}$) it is possible to calculate the apparent nC_9 density

of the confined hydrocarbon in MCM-22, which amounts to 0.522. This value differentiates form the density of liquid nC_9 at RT (*i.e.* 0.718) and indicates that the density of the confined hydrocarbon is lower than in the liquid phase. This allows to calculate the micropore volume from the nC_9 adsorption isotherms, which amounts to 0.176 mL g^{-1} (at $P/P_0 = 0.019$), which compares rather well to the micropore volume deduced from the N_2 isotherm. It is to note that for the adsorption of such hydrocarbons at RT the development of the adsorbate monolayer on the external surface initiates only once micropores are completely filled, which thus allows to read the micropore volume directly from the isotherm.[21]

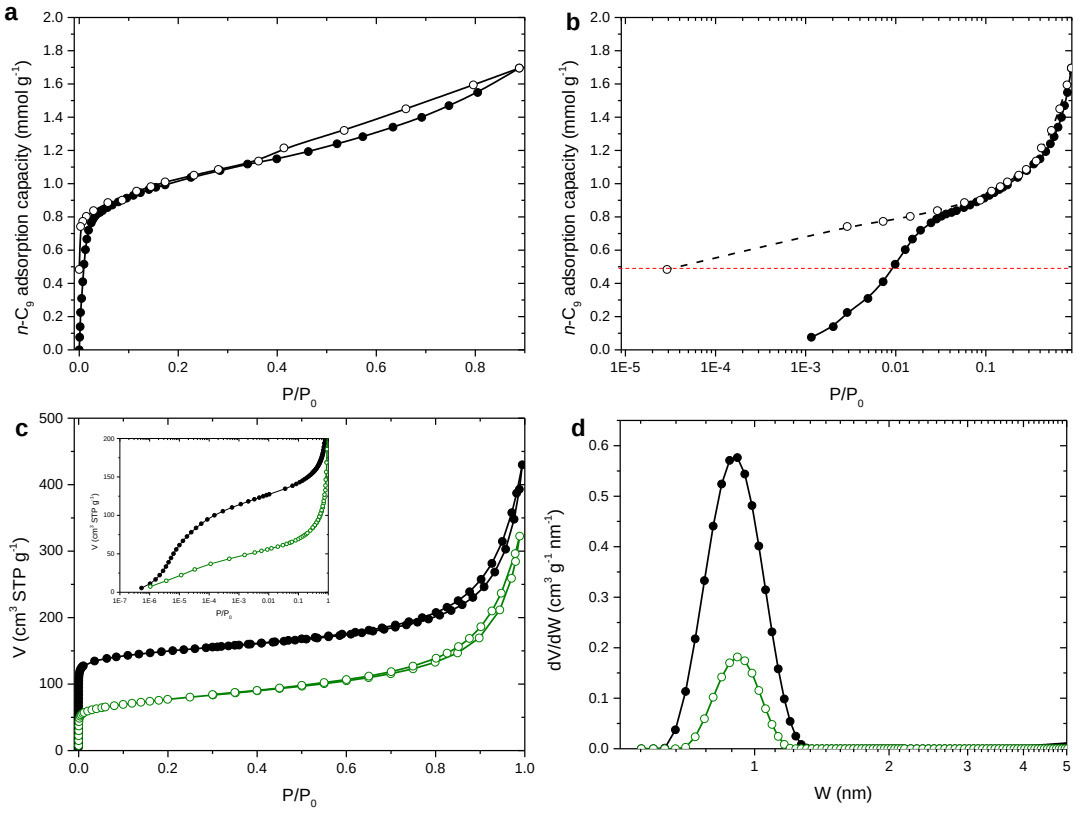

Figure 1. a) *n*-Nonane adsorption (full symbols) and desorption (empty symbols) isotherm at RT on MCM-22. b) *n*-Nonane isotherm with logarithmic P/P_0 scale allowing for a more detailed view of the micropore range. The dashed red line indicates the amount of nC_9 that is retained in the sample after outgassing at $1x10^{-4}$ mbar during 24 h. c) Nitrogen physisorption isotherms at 77 K on MCM-22 (black, full symbols) and on nC_9 retaining MCM-22 (green, empty symbols). The insert presents the isotherms with logarithmic P/P_0 scale. d) DFT pore size distribution achieved from the nitrogen physisorption isotherms at 77 K of MCM-22 and MCM-22-nC_9.

The incomplete desorption of nC$_9$ from MCM-22 at RT can be explained by its high physisorption energy resulting in a high energy barrier for its desorption from certain micropores. The TGA of MCM-22-nC$_9$ allows to observe that the desorption of nC$_9$ only initiates at temperatures above 120 °C (**Figure S2**). For medium pore zeolites (10-MRs), such as ZSM-5 (MFI structure), the adsorption of nC$_9$ is irreversible in micropores at RT.[22] The adsorption nC$_9$ hence allows to block completely the micropore volume ZSM-5, which permits to achieve important insights as far as textural properties are concerned.[21] Whilst ZSM-5 features a microporous system of interconnected 10-MRs, the porous structure of MCM-22 is more complex as it is composed of three distinct porous networks which can be distinguished as follows (**Scheme 1**):

A: 2D sinusoidal 10-MR channels (0.40 x 0.59 nm).

B: Supercages (0.71 x 1.82 nm), which are connected in the *ab*-plane through non-circular 10-ring apertures (0.40 x 0.54 nm). The supercages are hence only accessible through the narrow 10-MRs.

C: Hemicages (cups) featuring 12-MR openings (0.71 nm) of 0.70 nm depth.

By comparing the micropore volume of MCM-22 with that of MCM-22-nC$_9$ the nitrogen accessible micropore volume fraction (φ_{N_2}) can be calculated by:

$$\varphi_{N_2} = \frac{\mathrm{V_{micro}\ of\ } n\mathrm{C_9\ retaining\ sampe}}{\mathrm{V_{micro}\ of\ pristine\ sample}} \qquad (1)$$

For MCM-22 a φ_{N_2} value of 0.28 was achieved indicating that less than 1/3 of the micropore volume is accessible to N_2 on the nC$_9$ retaining sample. As nC$_9$ adsorption in ZSM-5 micropores is totally irreversible at RT, it can be assumed that all of the micropore systems that are connected through 10-MR openings in MCM-22 (hence pore systems A and B) are entirely blocked by nC$_9$ and do not allow the adsorption of N_2. This indicates that 28% of the

micropore volume of MCM-22 results from the hemicages at the external surface. This value confirms nicely to what was previously reported by Lawton *et al*.[1] The authors performed dynamic adsorption of 2,2,4-trimethylpentane (TMP) on MCM-22 at 54 °C and observed two distinct adsorption rates. A fast initial adsorption (67 µmol TMP g^{-1} $s^{-1/2}$) corresponding to 30% of the equilibrium capacity, followed by a second substantially slower rate (6 µmol TMP g^{-1} $s^{-1/2}$). The first was related to the adsorption within the hemicage volume.

Both MCM-22 and MCM-22-*n*C_9 present DFT pore size distributions centered at 0.9 nm (**Figure 1d**). For MCM-22-*n*C_9 the pore size distribution is yet narrower compared to MCM-22 and ranges from 0.70 - 1.15 nm and 0.60 - 1.35 nm, respectively. Indicating that *n*C_9 blocks the smallest pores (pore system A) and largest pores (pore system B).

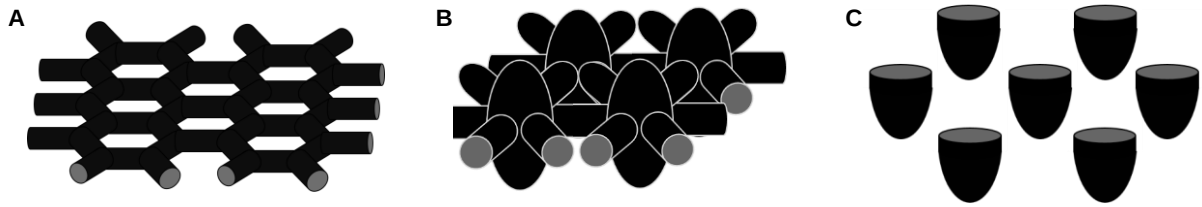

Scheme 1. Perspective view (artist's rendition) of the three pore systems in MCM-22. A: 2D sinusoidal 10-MR channels. B: Supercages connected through non-circular 10-MR apertures. C: Hemicages on crystal surface featuring 12-MR openings.

2.2 Textural properties of MCM-36

MCM-36 was achieved through pillaring of the swollen MCM-22(P) with TEOS. The X-ray powder patterns present the characteristic features expected for swMCM-22(P) and MCM-36 (**Figure S3**). Through swelling the characteristic 002 reflection (6.6 °2theta) disappears and the 001 (3.2 °2theta) shifts to lower angles (1.9 °2theta), confirming the expansion of the layers. Moreover the 003 reflection (6.1 °2theta) develops. All hkl reflections are further impacted through the treatment except for hk0 for which no change is observed. For example

the 101 and 102 reflections merge together, while 100, 220 and 310 remain unaffected. Upon pillaring a similar XRD pattern is achieved as for the swollen material.

Further evidence of pillaring was evidenced from TEM images of edge-oriented crystals, for which the separation of layers with ill-defined structures can be observed (**Figure 2**). The repeating distance between layers is approximately 4 nm which corresponds well to what was previously reported.[9]

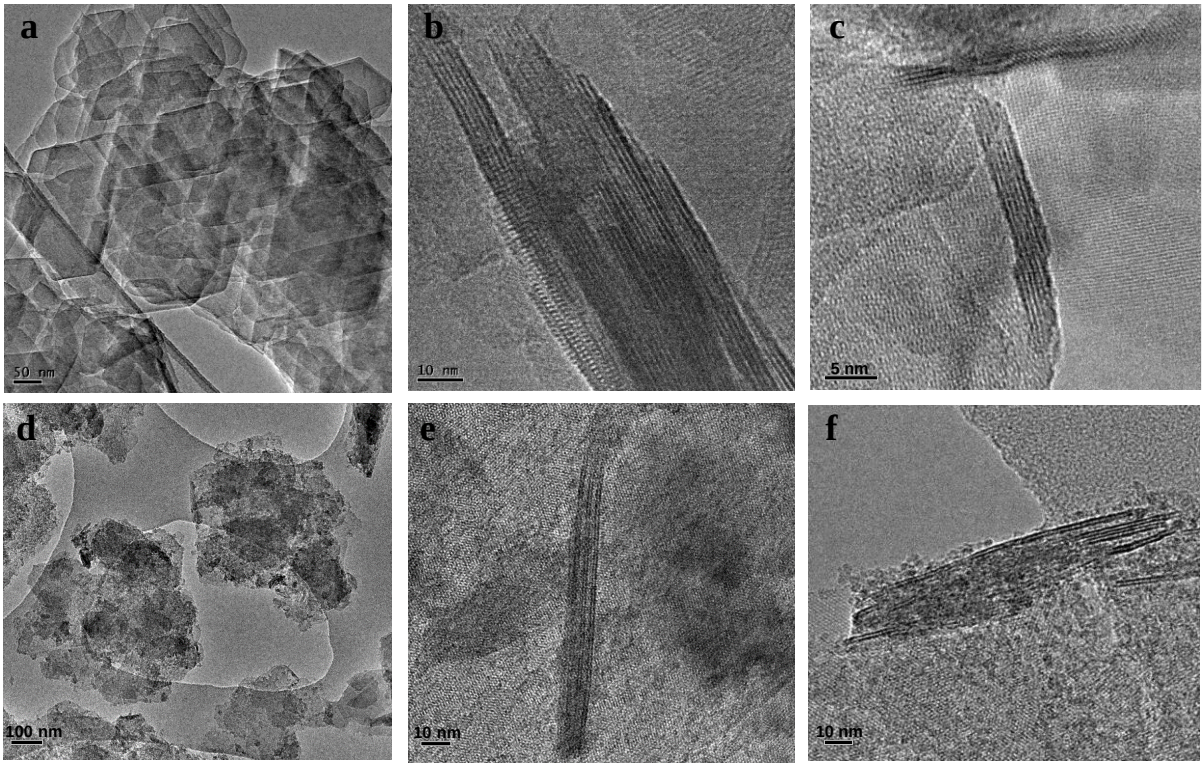

Figure 2. TEM images of MCM-22 (a-c) and MCM-36 (d-f).

The pillaring of the layers allows for the generation of small mesopores featuring a narrow size distribution, centered at 2.5 nm and a mesoporous volume of 0.17 cm^3 g^{-1} (**Figure 3**, **Table 1**). The Si/Al ratio increases during pillaring from 15.2 (for MCM-22(P)) to 19.8 (for MCM-36), indicating a 1.3 times higher amount of Si ascribable to amorphous silica formation within the MCM-22 layers. This allows to rectify the amount of nitrogen uptake for

the calculation of the micropore volume, which amounts hence to 0.147 $cm^3\ g^{-1}$. A considerably lower micropore volume was achieved for the *n*C_9 retaining MCM-36 (0.046 $cm^3\ g^{-1}$). A φ_{N_2} of 0.31 was calculated for MCM-36, which is just slightly higher than what was calculated for MCM-22 (φ_{N_2} = 0.28). This is rather surprising as a higher amount of accessible hemicages would be expected for MCM-36. Yet, the DFT pore size distribution of the *n*C_9 retaining MCM-36 features significant differences to what was observed for MCM-22-*n*C_9. Here, two distinct micropore population centered at 0.74 and 1.10 nm can clearly be distinguished (**Figure 3b**). This observation indicates that the pillaring step impacts microporosity severely. During the pillaring process TEOS condenses with silanol groups at the entrance of the hemicages in order to form the interlayer-pillars. This most probably modifies the openings of the hemicages, hence their accessibility. Next to forming pillars, one TEOS molecule is susceptible to condense two layers through just one silica species (single Si-pillar), this results in larger micropores, which explains the observed population of larger micropores. Such pillaring defaults can clearly be identified through careful observation of edge-on oriented crystals from TEM images (**Figure 2f**).

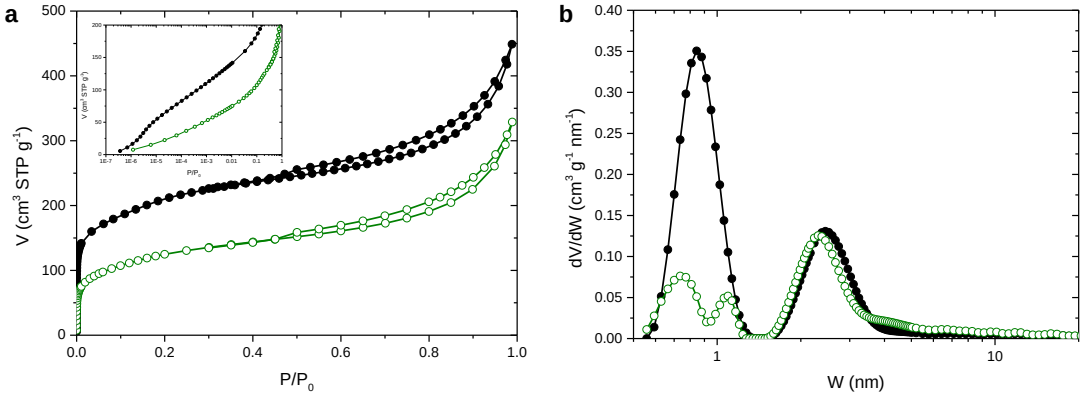

Figure 3. a) Nitrogen physisorption isotherms at 77 K on MCM-36 (black, full symbols) and on *n*C_9 retained MCM-36 (green, empty symbols). b) DFT pore size distribution of nitrogen physisorption isotherms at 77 K of MCM-36 (black, full symbols) and *n*C_9 retaining MCM-36 (green, empty symbols).

Hence, whilst tailored mesopores and increased BET surface area are achieved during pillaring, indicating successful enlargement of the interlayer space, the accessibility to hemicages only increases by 3% (**Figure 5**).

2.3 Hierarchical MCM-22 based materials through desilication

A series of hierarchical MCM-22 based materials were prepared based on desilication processes of the as-synthetized MCM-22(P), the calcined MCM-22 and the swollen swMCM22(P) materials (**Scheme 2**). The X-ray patterns indicate that all of the achieved materials present characteristic peaks related to the connected 3D MCM-22 structure (**Figure S4**). The patterns further confirm the absence of any amorphous material that could result from desilication. The pore size distributions derived from the nitrogen physisorption isotherms (**Figure 4 and S4**) indicate that the amount of intracrystalline mesopores depends importantly on which MCM-22 type material the treatment was performed. Highest mesopore volume developed for the surfactant-assisted desilication of MCM-22 (0.248 $cm^3\ g^{-1}$) for which a 2 M solution of NaOH was used. This sample further presents a large mesopore size distribution ranging from 2 - 10 nm. It is to note that the treatment with 0.2 M NaOH in the absence of the surfactant leads to complete amorphization of the sample, which explains why in these cases treatments were performed with 0.1 M NaOH. Alkaline treatment of calcined MCM-22 allows for the generation of mesopore volume (0.050 $cm^3\ g^{-1}$), (**Table 1**). For the as-synthetized MCM-22(P) the alkaline treatment merely allows for the development of some larger mesopores (> 7 nm). The Si/Al ratio of the hierarchical samples decreases with reducing micropore volume (**Figure 4b**). The tendency indicates that desilication in MCM-22 is limited and Si/Al ratios of lower than 8 cannot be achieved, due to dissolution of the zeolite.

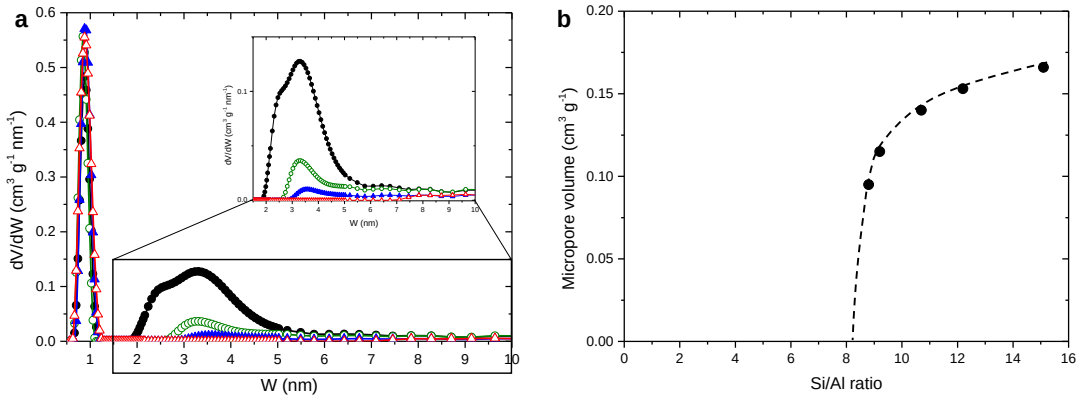

Figure 4. a) DFT pore size distribution of MCM-22-CTAB/OH (black, full circles), MCM-22-OH (green, empty circles), swMCM-22(P)-OH (blue, full triangles), MCM-22(P)-OH (red, empty triangles). b) Micropore volume as a function of the Si/Al ratio of hierarchical MCM-22 based samples.

Figure 5 compares the normalized micropore volume, specific BET surface area and the accessible micropore volume fraction by taking the results obtained by MCM-22 as benchmark (**Table 1**). For all of the hierarchical samples the micropore volume is lower with respect to MCM-22. The strongest reduction of micropore volume is evidenced for the alkaline treatment of MCM-22 (*i.e.* MCM-22-OH). This is further the sample for which φ_{N_2} is lowest, indicating that only 18% of the micropore volume is accessible in the *n*C_9 retaining sample. This suggests that the alkaline treatment on calcined MCM-22 preferentially destroys the 12-MR cups on the external surface of the crystals. From the TEM images it is indeed possible to observe that the developed mesopores do not traverse the integrity of the zeolite crystals (**Figure 6**). For this sample the value of S_{BET} only slightly decreases compared to the parent MCM-22, which highlights that the simple comparison of BET surface areas for the deduction of hierarchization quality leads to mayor misconstruction of textural properties. The use of the BET surface area for the description of textural properties for zeolites and especially hierarchical zeolites has repeatedly been questioned.[21,23]

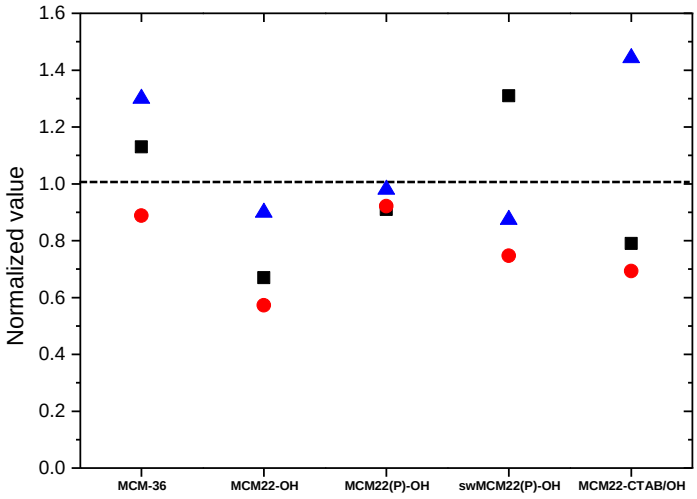

Figure 5. Normalized micropore volume (red circles), specific BET surface area (blue triangles) and accessible volume fraction (black squares) for hierarchical MCM-22 based materials.

For the surfactant-assisted desilication of calcined MCM-22 an important rise in BET surface area is observed. Notwithstanding, micropore volume reduces by approximately 30%. The accessible micropore volume fraction slightly decreases indicating that the hemicages on the external crystal surface are preferentially removed during the treatment.

The alkaline treatment on the as-synthetized MCM-22(P) only marginally impacts the textural properties of the material, which are hence comparable to those inferred for MCM-22. A slight decrease in micropore volume and accessible micropore volume fraction is observed as some larger mesopores develop, which can clearly be observed from the TEM images (**Figure 6f**). It can hence be assumed that the presence of the structure directing agent in the precursor material acts as crystal 'protecting' agent.[24]

The swollen swMCM-22(P) precursor is the only sample for which the accessible micropore volume fraction substantially increases upon alkaline treatment (φ_{N_2} = 0.36), whilst micropore

volume slightly reduces compared to MCM-22. This indicates that porosity on the external surface is preferentially maintained during the treatment. Indeed, from the TEM images the development of pores within the flat crystals rather than on the outer surface can be deduced (**Figure 6h**). This might be related to the presence of CTAB at the interlayer, which in combination with the base leads to the development of surfactant-templated mesopores that are preferentially located within the crystals after calcination.

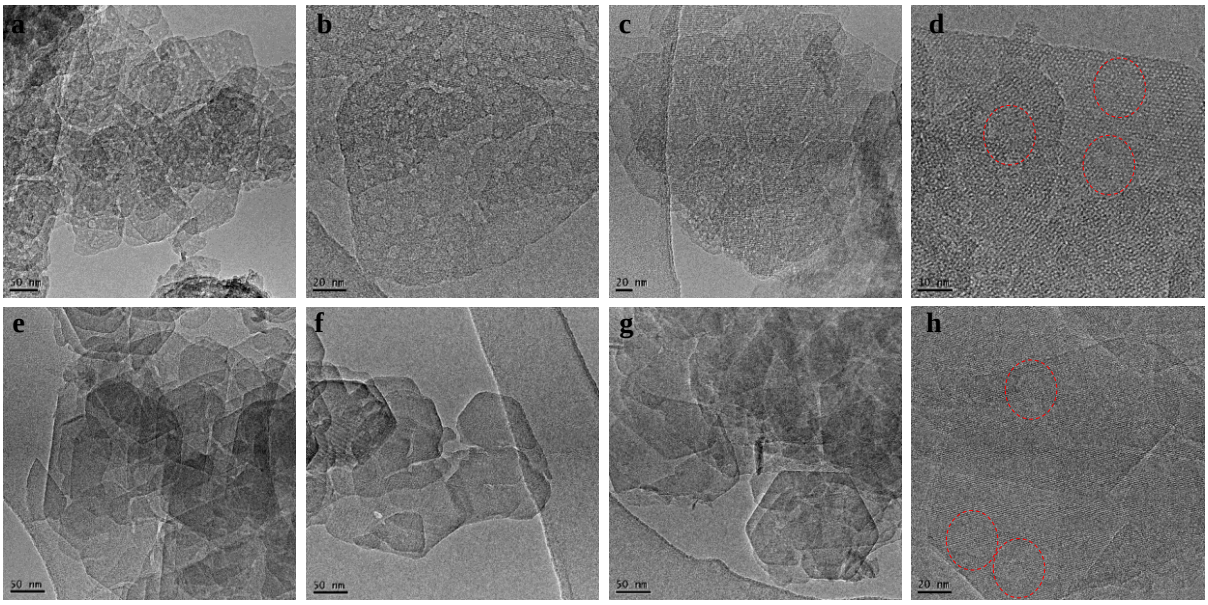

Figure 6. TEM images of hierarchical MCM-22 based materials: MCM-22-OH (a,b), MCM-22-CTAB/OH (c,d), MCM(P)-22-OH (e,f) and swMCM(P)-22 (g,h).

Table 1. Textural properties of MCM-22 based materials.

	V_{micro} (cm^3 g^{-1})	S_{BET} (cm^3 g^{-1})	V_{meso}[a] (cm^3 g^{-1})	φ_{N_2}
MCM22	0.166	553	0	0.28
MCM36	0.147	719	0.169	0.32
MCM22-OH	0.095	497	0.050	0.18
MCM22-CTAB/OH	0.115	798	0.248	0.22
MCM22(P)-OH	0.153	542	0.003	0.25
swMCM22(P)-OH	0.140	483	0.014	0.36

[a]Corresponding to the intracrystalline mesopore volume deduced by cumulative DFT volume at 5 nm and subtracting V_{micro}.

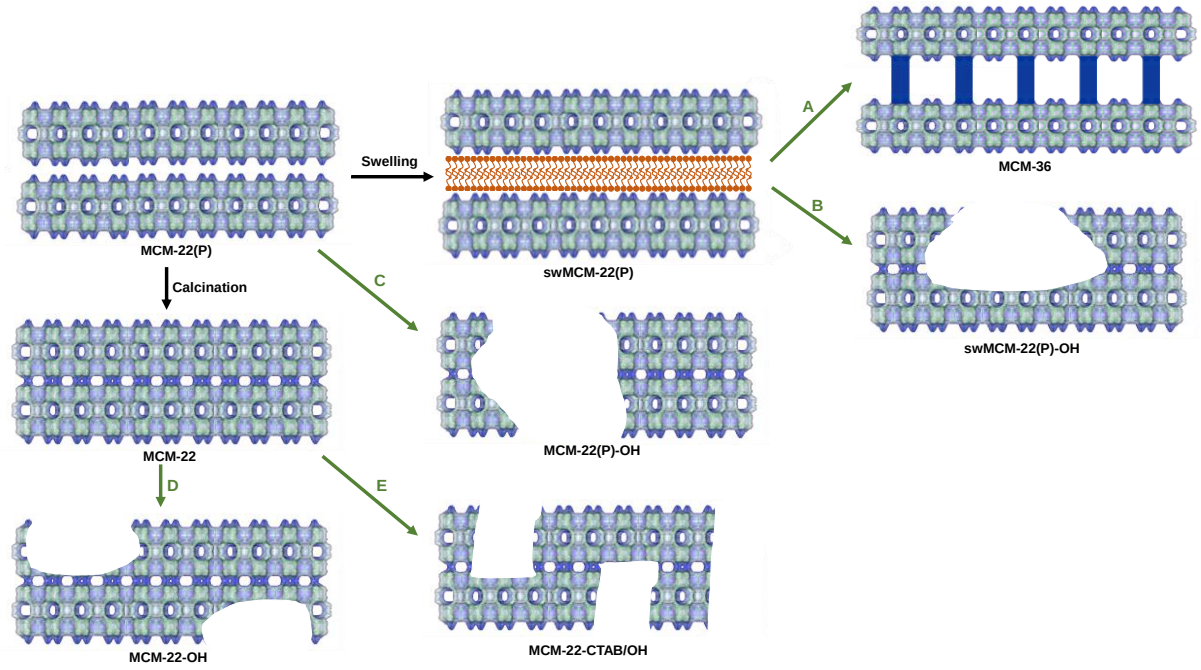

Scheme 2. Schematic representation of the different MCM-22 based materials used in this study. The green arrows indicate hierarchization treatments. A: Self pillaring of the swollen MCM-22(P) using TEOS. B: Treatment of swMCM-22(P) with 0.1 M NaOH. C: Treatment of MCM-22(P) with 0.1 M NaOH. D: Treatment of MCM-22 with 0.1 M NaOH. E: Treatment of MCM-22 with 0.2 M NaOH and 0.05 M CTAB solution.

3. Conclusion

Whilst zeolite hierarchization is often stressed in terms of increased BET surface area and preservation of microporosity, the impact of such treatments on distinct pore systems is mostly neglected. Through characterizing hierarchical MCM-22 based materials and comparing their properties with those of the *n*-nonane retaining counterparts important evidence on the impact of the hierarchization treatment on the accessible micropore volume was evidenced. As such, it was proved that though substantial growth of BET surface area and interlayer-mesopore volume in MCM-36 the accessible micropore volume fraction hardly increases compared to calcined MCM-22. This indicates that the pillaring only marginally allows to increase accessibility to hemicages. As far as desilication treatments are concerned, most lead to a reduced accessible micropore volume fraction, indicating that desilication

preferentially destroys hemicages on the crystal surface. For the swollen MCM-22(P) precursor desilication yet allows for a substantial increase in the accessible micropore volume fraction, which is probably related to the presence of the cationic surfactant in the interlayer volume that hence allows to induce surfactant-templating from the inside of the crystal.

4. Experimental section

4.1 Materials

Sodium hydroxide (>97%, Fisher Scientific), Tetrapropylammonium hydroxide (TPAOH, 40 wt% in water, Alfa Aesar), Tetraethylorthosilicate (TEOS, 98%, Fisher Scientific), Sodium aluminate (technical, Fisher Scientific), Hexamethyleneimine (HMI, 99%, Sigma-Aldrich), Hexadecyltrimethylammonium bromide (CTAB, 98%, Sigma-Aldrich) and Aerosil 200® (Evonik) were purchased and used as received.

4.2 Synthesis of materials

4.2.1 Synthesis of MCM-22(P)

The lamellar precursor MCM-22(P) was synthesised following the method developed by Corma *et al.*[25] for which 0.6 g of NaOH and 0.92 g of $NaAlO_2$ were dissolved in 124.2 g of demineralized water. After stirring for 1 h at RT, 8.65 mL of HMI were added to the solution followed by 9.23 g of Aerosil 200®. After 2 h under vigorous stirring, the resulting gel was transferred to a 250 mL Teflon-lined stainless steel autoclave. The hydrothermal treatment was carried out during 7 days at 150 °C under constant rotation (60 rpm). After recovering, washing and drying, a white powder was obtained corresponding to MCM-22(P).

4.2.2 Synthesis of MCM-22

In order to achieve MCM-22 the precursor material MCM-22(P) was calcined at 550 °C (1 °C min^{-1}) under air for 6 h in a muffle furnace.

4.2.3 Preparation of the CTAB swollen precursor swMCM-22(P)

The swelling of the precursor material was achieved using the method described by Maheshwari *et al.*[26] Typically, 4 g of MCM-22(P) was suspended in 16 g of demineralized water. Then 68.9 g of an aqueous solution of CTAB (29 wt%) was added to the mixture followed by 24.4 g of TPAOH (40 wt% in water). After 16 h under stirring at room temperature, a white mixture was obtained and the swollen material was recovered by centrifuged. The recovered solid was abundantly washed with hot absolute ethanol in order to remove the excess of CTAB and dried at 90 °C overnight. The obtained white powder was named swMCM22-(P).

4.2.4 Synthesis of the pillared material MCM-36

The swollen swMCM-22(P) was pillared using the procedure developed by Chlubná *et al*.[27] Typically, 0.5 g of swMCM-22(P) were combined with 15 g of TEOS and stirred overnight at 90 °C. The solid phase was recovered by centrifugation. After centrifugation the tube was reversed and kept upside down during 24 h at RT in order to remove the excess of TEOS. The solid was then suspended in 20 mL of double distilled water, stirred overnight and recovered by centrifugation before drying at 80 °C for 12 h. MCM-36 was obtained after calcination of the material for 6 h at 550 °C (1 °C min^{-1}) under air.

4.2.5 Hierarchization of MCM-22 based materials through desilication

Hierarchical MCM-22 based materials were achieved by alkaline treatment of MCM-22(P), MCM-22 and swMCM-22(P). A 0.1 M NaOH (56 mL) was heated in a closed vessel under constant stirring at 50 °C before adding 0.6 g of the MCM-22 based material. Stirring at this temperature was continued for 45 min before quenching the reactor in an ice bath. The mixture was centrifuged and the remaining solid washed with distilled water until neutral pH. The solids were dried at 80 °C for 12 h and then calcined at 550 °C (1 °C min^{-1}) for 6 h under air. The obtained materials were named MCM-22(P)-OH, MCM-22-OH and swMCM-22(P)-OH.

Surfactant-assisted desilication of MCM-22 was achieved by mixing 12 mL of a 0.1 M aqueous CTAB solution and 12 mL of a 0.2 M NaOH solution. After heating to 70 °C in a closed vessel 0.6 g of MCM-22 were added and kept at this temperature for 2 h under constant stirring. After centrifugation and washing with distilled water, the white solid was dried at 80 °C during 12 h prior to calcination at 550 °C (1 °C min^{-1}) for 6 h under air. The obtained material was named MCM-22-CTAB/OH.

4.3 Methods

n-Nonane adsorption and desorption isotherms were recorded at 298 K by thermogravimetry on a SETARAM microbalance. The samples (30 mg) were outgassed under secondary vacuum at 573 K for 12 h. The sorbate pressure was increased stepwise (interval of 0.010 mbar for low relative pressures) and stabilized until reaching equilibrium. After measuring the desorption the samples were outgassed under secondary vacuum for 24 h. The recovered materials were designated *n*-nonane retaining samples.

Nitrogen physisorption isotherms were achieved at 77 K using a Micromeritics 3FLEX instrument. Calcined samples were outgassed under secondary vacuum for 12 h at 623 K and

n-nonane retaining samples for 12 h at RT prior to nitrogen physisorption. Specific surface area was calculated by applying the Brunauer–Emmett–Teller (BET) equation on the linear zone of the BET plot using the Rouquerol criterion.[23] Micropore volume was calculated from *t*-plots using the reference described by Galarneau *et al*.[28] Nitrogen physisorption isotherms on *n*-nonane retaining samples were corrected by taking the wt% of adsorbed *n*-nonane into consideration. The amount of *n*-nonane in the sample correlates with the amount of inaccessible pore volume as depicted in **Figure S1**.

Transmission Electronic Microscopy (TEM) was performed using a JEOL 2100 instrument (operated at 200 kV with a LaB_6 source and equipped with a Gatan Ultra scan camera). X-ray powder diffraction patterns were recorded using a PANalytical Empyrean X-ray diffractometer using CuKα radiation (0.154059 nm), for 2theta ranging from 1-5° in the low angle range and 5-40° for large angles. Scan speed was fixed at 0.008° min^{-1}. The elemental Si/Al ratios were determined by using ICP-OES analysis, using a Perkin Elmer Optima 2000 DV instrument.

Supporting Information

Further materials characterization, including X-ray powder diffraction patterns, nitrogen physisorption isotherms and TGA and is available as supporting information.

Acknowledgements

The authors acknowledge financial support from the European Union (ERDF) and "Région Nouvelle Aquitaine".

References

[1] S. L. Lawton, M. E. Leonowicz, R. D. Partridge, P. Chu, M. K. Rubin, *Microporous Mesoporosu Mater.* **1998**, *23*, 109.

[2] T. F. Degnan, C. M. Smith, C. R. Venkat, *Appl. Catal. A* **2001**, *221*, 283.

[3] J. S. Beck, A. B. Dandekar, T. F. Degnan, Aromatic Alkylation: Towards Cleaner Processes, in: M Guisnet, J.-P. Gilson (Eds.); Zeolites for Cleaner Technologies, catalytic Science Series, Vol. 3, Imperial College Press, London, **2002**, pp. 230-237.

[4] S. Laforge, D. Martin, M. Guisnet, *Microporous Mesoporous Mater*. **2004**, *67*, 235.

[5] W. J. Roth, MCM-22 zeolite family and the delaminated zeolite MCM-56 obtained in one-step synthesis, in: J. Čejka, N. Žilková, P. Nachtigall (Eds.); Molecular Sieves: From Basic Research to Industrial Applications, Stud. Surf. Sci. Catal. Vol. 158, Part A, Elsevier, New York, **2005**, pp. 19-26.

[6] M. E. Leonowicz, J. A. Lawton, S. L. Lawton, M. K. Rubin, *Science* **1994**, *264*, 1910.

[7] S. L. Lawton, A. S. Fung, G. J. Kennedy, L. B. Alemany, C. D. Chang, G. H. Hatzikos, D. N. Lissy, M. K. Rubin, H.-K. C. Timken, S. Steuernagel, D. E. Woessner, *J. Phys. Chem.* **1996**, *100*, 3788.

[8] A. Corma, V. Fornes, S. B. Pergher, Th. L. M. Maesen, J. G. Buglass, *Nature* **1998**, *396*, 353.

[9] W. J. Roth, C. T. Kresge, J. C. Vartuli, M. E. Leonowicz, A. S. Fung, S. B. Mc Cullen, MCM-36: The first pillared molecular sieve with zeoliteproperties, in: H/ K. Beyer, H. G. Karge, I. Kiricsi, J. B. Nagy (Eds.) ; Catalysis by Microporous Materials, Stud. Surf. Sci. Catal. Vol. 94, Elsevier, New York, **1995**, pp. 301-308.

[10] A. Sachse, J. Garcia Martinez, *Chem. Mater*. **2017**, *29*, 3827.

[11] M. Hartmann, A. G. Machoke, W. Schwieger, *Chem. Soc. Rev.* **2016**, *45*, 3313.

[12] L. Lakiss, F. Ngoye, C. Canaff, S. Laforge, Y. Pouilloux, Z. Qin, M. Tarighi, K. Thomas, V. Valtchev, A. Vicente, L. Pinard, J.-P. Gilson, C. Fernandez, *J. Catal.* **2015**, *328*, 165.

[13] P. A. Jacobs, M. Dusselier, B. F. Sels, *Angew. Chem. Int Ed.* **2014**, *53*, 8621.

[14] A. van Miltenburg, J. Pawlesa, A. M. Bouzga, N. Žilková, J. Čejka, M. Stöcker, *Top. Catal.* **2009**, *52*, 1190.

[15] K. Liua, S. Xiea, H. Weia, X. Lia, S. Liua, L. Xu, *Appl. Catal. A* **2013**, *468*, 288.

[16] V. Machado, J. Rocha, A. P. Carvalho, A. Martins, Appl. Catal. A **2012**, *445–446*, 329.

[17] N. Gao, S. Xie, S. Liu, W. Xin, Y. Gao, X. Li, H. Wei, H. Liu, L. Xu, *Microporous Mesoporous Mater*. **2015**, *212*, 1.

[18] J. Fernandes Gomes, A. Sachse, J. R. Gregório, K. Bernardo-Gusmão, A. J. Schwanke, *Cryst. Growth Des.* **2020**, *20*, 178.

[19] M. V. Rodrigues, C. Okolie, C. Sievers, L. Martins, *Cryst. Growth Des.* **2019**, *19*, 231.

[20] Y. Wang, T. Yokoi, S. Namba, J. N. Kondo, T. Tatsumi, *J. Catal.* **2016**, *333*, 17.

[21] I. Batonneau-Gener, A. Sachse, *J. Phys. Chem. C* **2019**, *123*, 4235.

[22] Y. Grillet, P. L. Llewellyn, M. B. Kenny, F. Rouquerol, J. Rouquerol, *Pure Appl. Chem.* **1993**, *65*, 2157.

[23] J. Rouquerol, P. Llewellyn and F. Rouquerol, *Stud. Surf. Sci. Catal.* **2007**, *160*, 49.

[24] D. Verboekend, J. Pérez-Ramírez, *Catal. Sci. Technol.* **2011**, *1*, 879.

[25] A. Corma, C. Corell, J. Pérez-Pariente, *Zeolites* **1995**, *15*, 2.

[26] S. Maheshwari, E. Jordan, S. Kumar, F.S. Bates, R.L. Penn, D.F. Shantz, M. Tsapatsis, *J. Am. Chem. Soc*. **2008**, *130*, 1507.

[27] P. Chlubná, W. J. Roth, A. Zukal, M. Kubů, J. Pavlatova, *Catal. Tod.* **2012**, *179*, 35.

[28] A. Galarneau, D. Mehlhorn, F. Guenneau, B. Coasne, F. Villemot, D. Minoux, C. Aquino, J.-P. Dath, *Langmuir* **2018**, *34*, 14134.

A new methodological approach is presented based on contrasting nitrogen physisorption isotherms at 77 K of hierarchical MCM-22 based materials and of the *n*-nonane retaining counterparts, which allows for calculating the accessible micropore volume fraction (φ_{N_2}) and hence permits for defining hierarchization quality from a novel point of view.

Alexander Sachse, Thibaud Aumond, Julie Rousseau and Isabelle Batonneau-Gener*

Impact of hierarchization on the textural properties of MCM-22 based zeolites

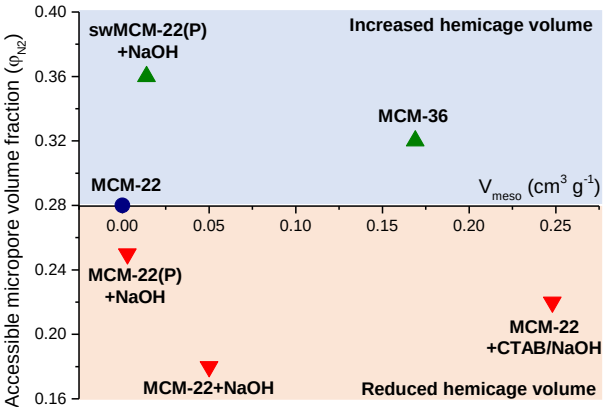

Supporting Information

Impact of hierarchization on the textural properties of MCM-22 based zeolites

Alexander Sachse, Thibaud Aumond, Julie Rousseau, Isabelle Batonneau-Gener*

Institut de Chimie des Milieux et Matériaux de Poitiers (IC2MP), Université de Poitiers – UMR 7285 CNRS, UFR SFA, Bat. B27, 4 rue Michel Brunet, TSA 51106, 86073 Poitiers, Cedex 9, France.

*corresponding author: alexander.sachse@univ-poitiers.fr

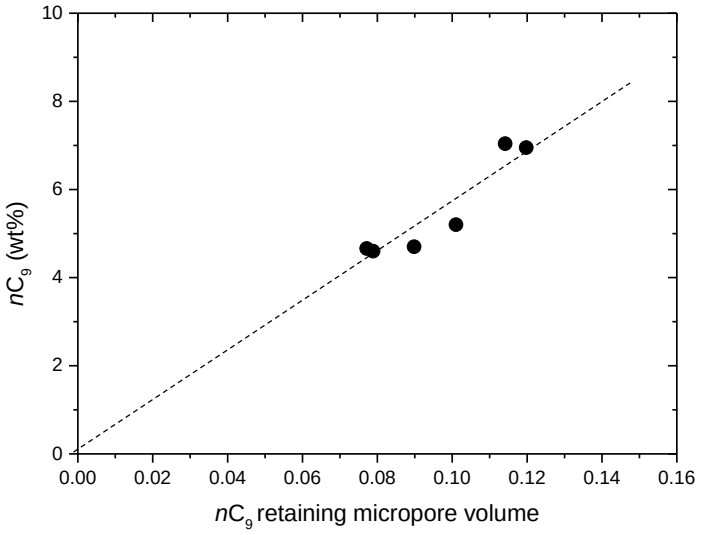

Figure S1. *n*-Nonane wt% as a function of the micropore volume of *n*-nonane retaining samples.

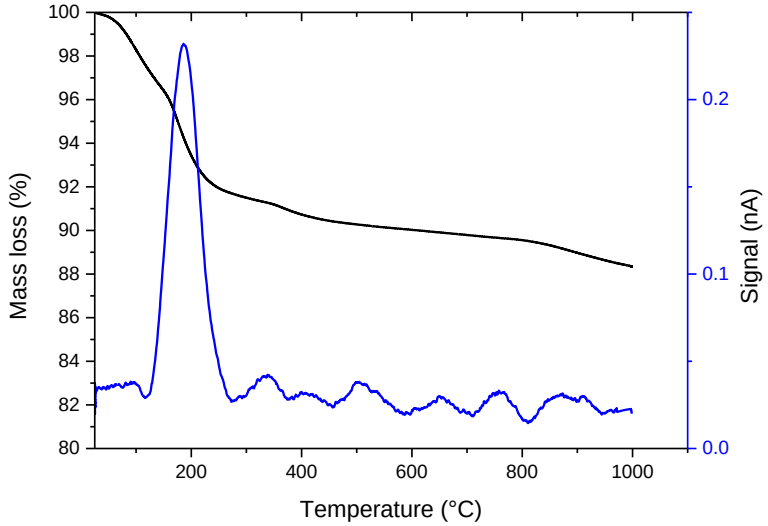

Figure S2. TGA mass loss curve of MCM-22-*n*C_9 (black) and MS signal corresponding to m/z = 128 (blue).

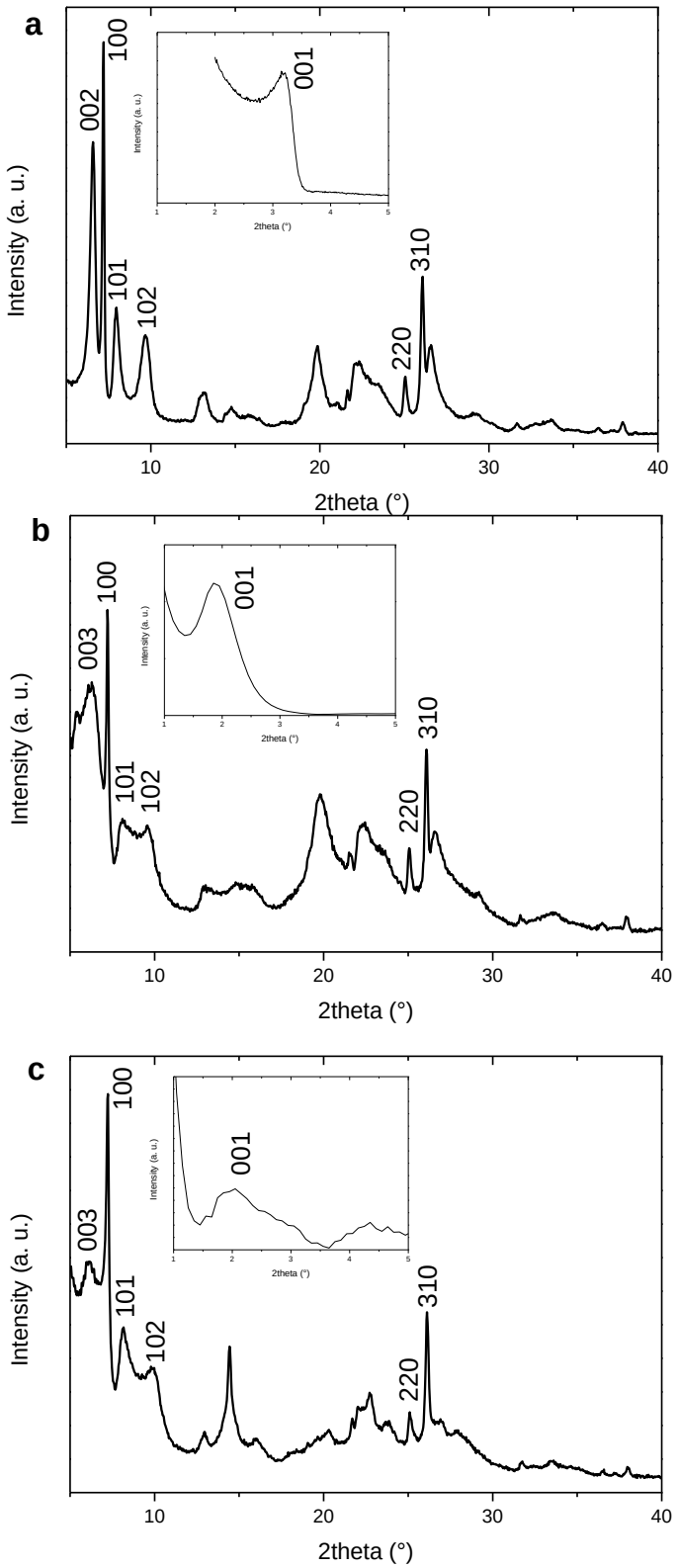

Figure S3. X-ray powder diffraction patterns of MCM-22(P), swMCM-22(P) and MCM-36. Selected reflections are identified with hkl indices. The inserts present the low angle X-ray powder patterns.

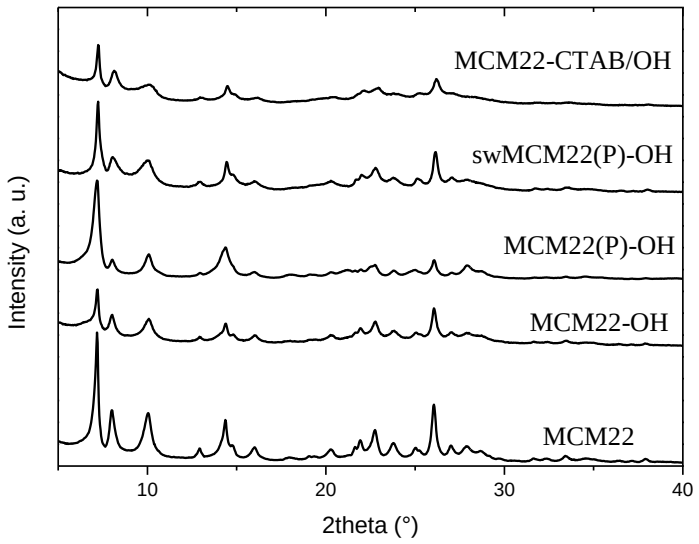

Figure S4. X-ray powder diffraction patterns of hierarchical MCM-22 based materials.

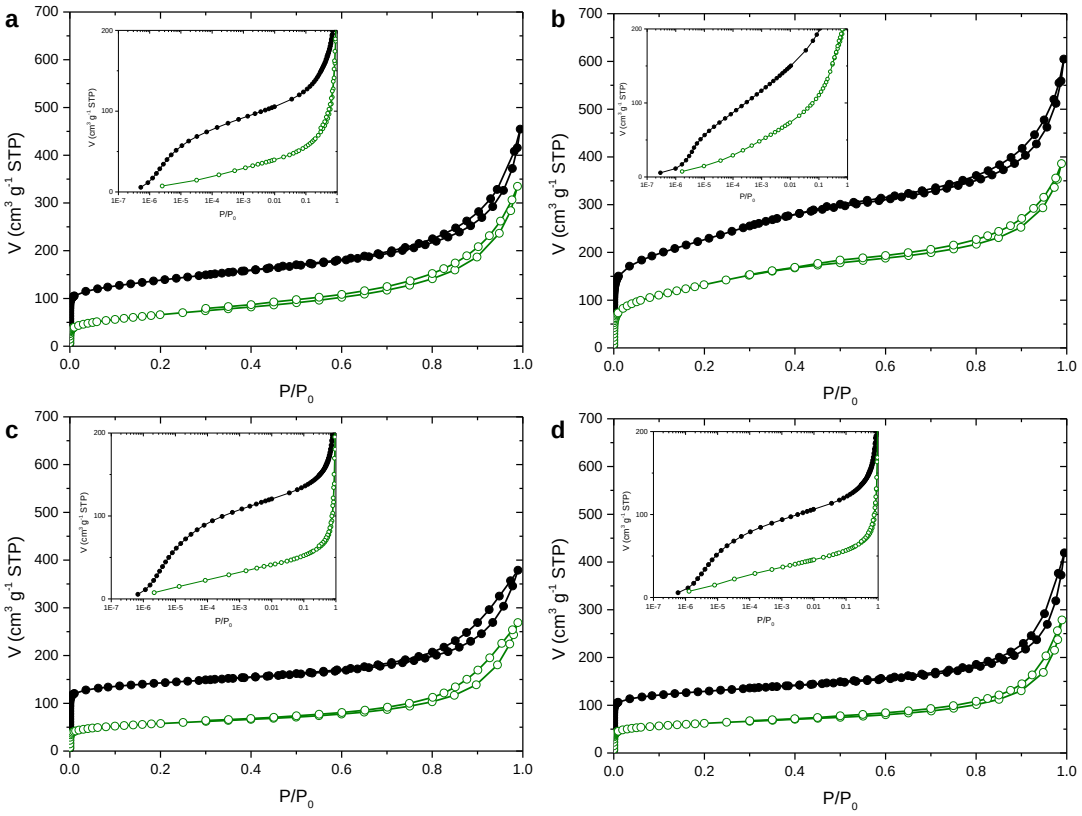

Figure S5. Nitrogen physisorption isotherms at 77 K of hierarchical MCM-22 based materials: MCM-22-OH (a), MCM-22-CTAB/OH (b), MCM(P)-22-OH (c) and swMCM(P)-22-OH (d).